Visible-Light Photocatalysis with WO_3/TiO_2 Nanocomposite Fiber Sponges Prepared via Solution Blow-Spinning Process

Jate Panichpakdee[1,*], Sarat Nuchapong[1,*], Busarin Noikaew[1,*],
Saengdeon Doungdaw[1,*], and Siriporn Larpkiattaworn[1,*]

Received April 14, 2020; Revised April 14, 2020; Accepted June 29, 2020

Abstract

Three-dimensional nanocomposite fiber sponges consisting of tungsten trioxide (WO_3) and titanium dioxide (TiO_2) as visible-light photocatalysts were successfully prepared by solution blow-spinning process in combination with a calcination process (450 °C). The precursor solution of tungstic acid (H_2WO_4)/tetrabutyl titanate ($Ti(OBu)_4$)/ polyvinyl pyrrolidone (PVP) with various molar percentage ratios of tungsten to Ti (i.e., 0.5, 1.0, 3.0, and 5.0) in 75/25 w/w mixture of ethanol and acetic acid were prepared and blown-spun. Smooth fiber morphologies and average fiber diameters in a range of 480 nm to 645 nm before calcination and 351 nm to 479 nm after calcination were observed by a scanning electron microscope (SEM). The presence of WO_3 within the nanocomposite fiber sponges was found by using X-ray diffractometer (XRD). The photocatalytic properties of the WO_3/TiO_2 nanocomposite fiber sponges were investigated by photocatalytic degradation of methylene blue solution under both UV- and visible-light radiation. Results showed that the WO_3/TiO_2 nanocomposite fiber sponges at molar percentage ratios of 5.0 exhibited the highest activity under both UV- and visible-light radiation.

Keywords: Photocatalyst, WO_3/TiO_2, Nanocomposite fiber sponges

Introduction

Titanium dioxide is one of the most popular photocatalysts which have been widely investigated because of its advantages such as non-toxicity, low cost, chemical stability, and high photocatalytic property (Li et al., 2005; Zhang et al., 2006; Ye et al., 2013) . Recently, it has been extensively used in a variety of fields, including air purification, self-cleaning surfaces, and water purification (Luevano-Hipolito et al., 2014; Elahifard et al., 2007; Wang and Lim, 2013). The photocatalytic activity mechanism of TiO_2 involved with converting solar energy to chemical energy by generating the photoinduced electrons and holes. As a result, superoxide radical anions and hydroxyl radicals generated from the reaction between the holes and water molecules could decompose organic matter (Zeng et al., 2007; Ismail & Bahnemann, 2011). However, the use of TiO_2 is still limited in some aspects due to its wide electronic band gap value of 3.2 eV, requiring only UV light to activate. Moreover, the rapid photo-generated electron-hole recombination rate of TiO_2 also reduces its photocatalytic activity (Hayden, Allam and El-Sayed, 2010; (Linsebigler, Lu and Yates, 1995).

To overcome these limitations, several previous researchers have paid attention to extend TiO_2 adsorption in the visible spectrum and to reduce recombination rate of photo-generated electron-hole pairs by doping with metals/non-metals, surface modification, loading of metal nanoparticles, and combing with other semiconductors such as CdS, Fe_2O_3, Bi_2O_3, WO_3, etc. The coupled semiconductor oxides have been widely reported to improve the photocatalytic activity, in comparison to that of individual semiconductors (Luevano-Hipolito et al., 2014; Laursen et al., 2012; Kment

[1] Thailand Institute of Scientific and Technological Research, Khlong Luang, Pathum Thani, 12120, Thailand
* Corresponding author. Email: Jate@tistr.or.th, Sarat@tistr.or.th, Busarin@tistr.or.th, Saengdeon@tistr.or.th, Siriporn@tistr.or.th

et al., 2017). Among them, WO_3 has attracted much attention for enhancing the photocatalytic activity of TiO_2, owing to its advantages such as low cost, smaller band gap (2.7 eV), and high stability in water (Yadav et al., 2017; Mugunthan, Saidutta and Jagadeeshbabu, 2018; Ofori et al., 2015).

Nowadays, nanofibers have received a great deal of attention in the field of environment such as air purification and water purification due to excellent characteristics such as high surface area to volume, and high porosity (Doshi and Reneker, 1995; Khil et al., 2003). Various WO_3/TiO_2 nanofibers, mostly based on electrospinning process, were reported (Chen et al., 2016; Chakornpradit, Phiriyawirut and Meeyoo, 2017; Szilagyi et al., 2013). However, the WO_3/TiO_2 nanofibers typically were manufactured in a flat form (two-dimensional or 2D). In this work, three-dimensional photocatalysts consisting of WO_3 and TiO_2 with various molar percentage ratios of tungsten to Ti (i.e., 0.5, 1.0, 3.0, and 5.0) prepared by solution blow-spinning process was investigated.

Experimental Procedure

Polyvinyl pyrrolidone (PVP; with a molecular weight about 1,300,000), tungstic acid (H_2WO_4; ≥99%), tetrabutyl titanate ($Ti(OBu)_4$; ≥97%), and methylene blue (MB; dry content ≥82%) were purchased from Sigma-Aldrich (Switzerland). Ethanol (99%) and acetic acid (99.8%) were purchased from Lab-Scan Asia (Thailand). All of the chemicals were of analytical grade and used without further purification.

As for the preparation of TiO_2 fiber sponges, the precursor solution of $Ti(OBu)_4$/PVP was prepared by a sol-gel method and blown-spun as previously described by Wang et al., 2017. Briefly, $Ti(OBu)_4$ and PVP with 2:1 mass ratio were mixed in a mixture of ethanol and acetic acid (75/25 w/w). The concentration of PVP in the solution was fixed at 7 wt%. The solution was continuously stirred using magnetic stirring for 6 h at room temperature, and then was blown-spun by using a specific coaxial needle under a gas pressure of 69 kPa (airflow velocity is about 21 m/s). The flow rate of the solution and the distance between the tip to the porous and air permeable-cage collector were set at 3 mL/h and 20 cm, respectively. After spinning, the $Ti(OBu)_4$/PVP fiber sponges were immediately calcined at 450 °C for 200 min in air. Finally, the fiber sponges were irradiated with UV radiation (12 W) for 2 h prior to further use.

As for the preparation of WO_3/TiO_2 nanocomposite fiber sponges, the preparation process was similar to that of TiO_2 fiber sponges, except that the H_2WO_4 with various molar percentage ratios of tungsten (W) to Ti (i.e., 0.5, 1.0, 3.0, and 5.0) was dispersed in 75/25 w/w mixture of ethanol and acetic acid under magnetic stirring for 48 h and sonicated in ice bath for 5 min prior to the addition of $Ti(OBu)_4$ and PVP.

The particle size of H_2WO_4 after dispersion in mixed solvent was observed by using Zetasizer Nano

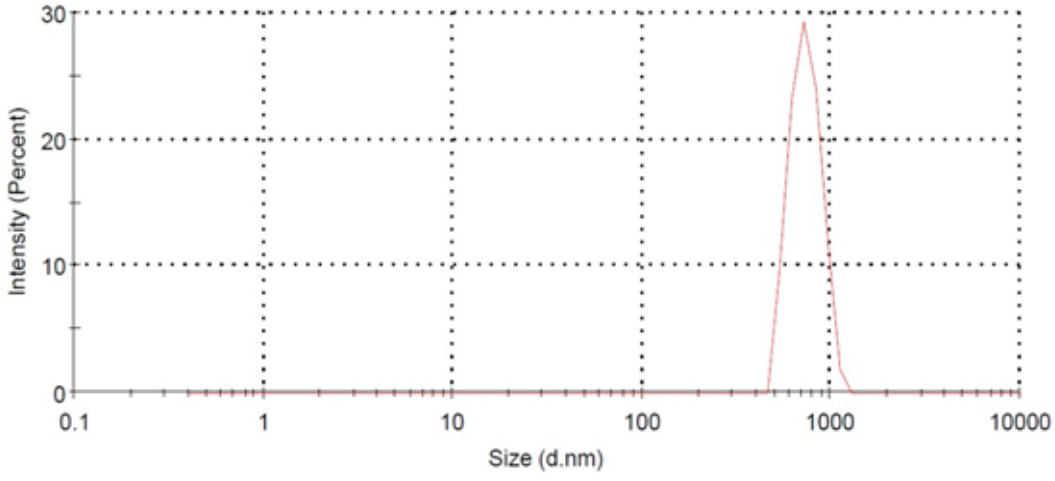

Figure 1. Particle size distribution of H_2WO_4 dispersed in 75/25 w/w mixture of ethanol and acetic acid.

ZS (Malvern Instrument). The morphology and size of the as-prepared fiber sponges were investigated using a Field Emission Scanning Electron Microscope (FE-SEM, JEOL, JSM-6304F). X-ray diffraction patterns of the as-prepared fiber sponges were recorded using a Rigaku SmarLab X-ray diffractometer (XRD).

The photocatalytic activity of the as-prepared fiber sponges was evaluated by monitoring degradation of MB under both UV- and visible-light radiation. The as-prepared fiber sponges were immersed (1g/L) in MB at a concentration of 10-5 mol/L, and irradiated with UV radiation (12W) or irradiated with visible-light radiation (LED lamp 18W). The changes of MB concentration during the test were measured by UV-Vis spectrometer (Shimadzu, UV-1700) at a wavelength of 660 nm.

Results and Discussion

H_2WO_4 dispersed in 75/25 w/w mixture of ethanol and acetic acid was evaluated in terms of particle size and size distribution as shown in Figure 1. The average diameter of H_2WO_4 prepared was 735.4 nm and the polydispersity index value of 0.353 were observed.

The prepared precursor solutions of $Ti(OBu)_4$/PVP and H_2WO_4/$Ti(OBu)_4$/PVP with various molar percentage ratios of tungsten to Ti (i.e., 0.5, 1.0, 3.0, and 5.0) were blown-spun by using a home-made equipment, which was assembled with an inner nozzle for allowing airflow and a concentric outer nozzle for injecting of prepared precursor solution as presented in Figure 2a. Under the pressure, the ejected precursor solution was rapidly stretched and solidified during traveling in air. As a result, the nanocomposite fiber sponges were collected in an air-permeable cage-like collector as represented in Figure 2b.

The morphologies of the $Ti(OBu)_4$/PVP and a series of H_2WO_4/$Ti(OBu)_4$/PVP fiber sponges with various molar percentage ratios of tungsten to Ti (i.e., 0.5, 1.0, 3.0, and 5.0) before and after calcination treatment at 450 ℃ for 200 min are presented in Figure 3. Before calcination treatment (figures on the left column), the

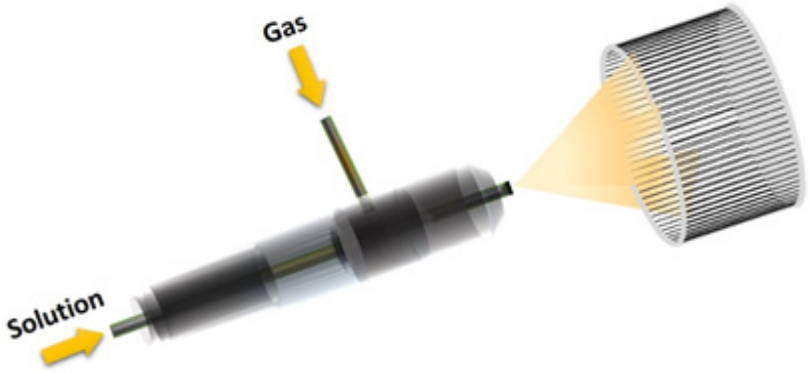

(a)

(b)

Figure 2. Schematic diagrams of (a) the solution blow-spinning and (b) photograph of the precursor H_2WO_4/$Ti(OBu)_4$/PVP fiber sponges obtained from the solution blow-spinning process.

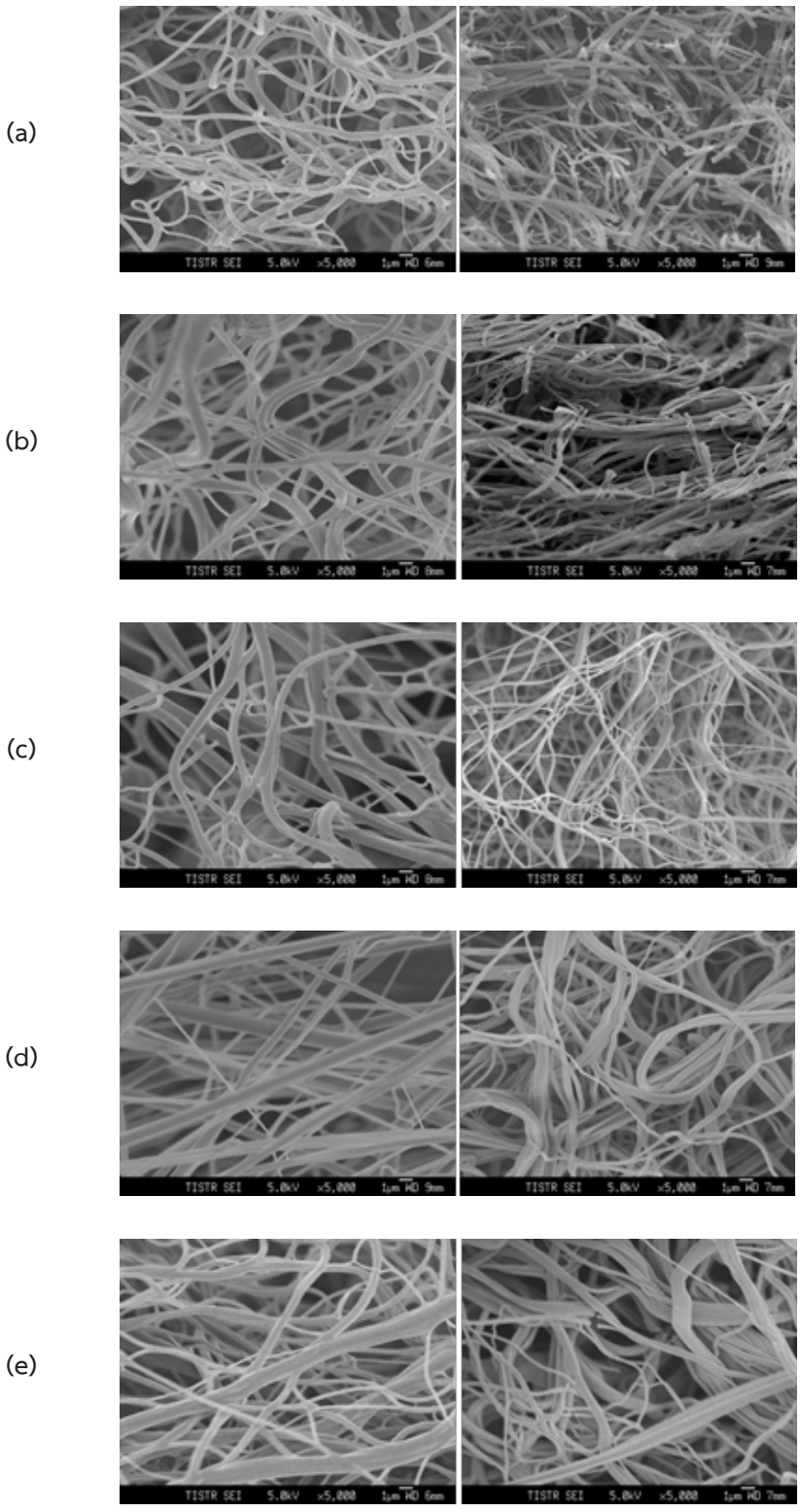

Figure 3. SEM images representing the surface morphologies of (a) $Ti(OBu)_4$/PVP fiber sponges, (b-e) the H_2WO_4/$Ti(OBu)_4$/PVP fiber sponges of tungsten to Ti molar ratios 0.5, 1.0, 3.0, and 5.0, respectively. Left column presents the fiber before calcination and right column presents the fibers after calcination at 450 °C for 200 min.

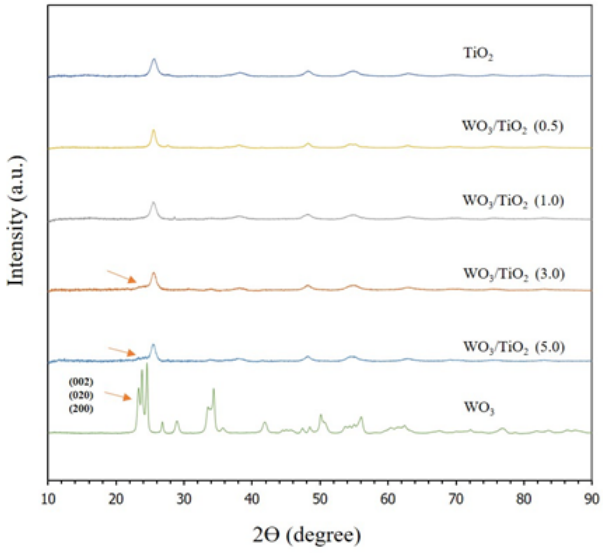

Figure 4. XRD patterns of TiO_2 fiber sponges and the WO_3/TiO_2 fiber sponges after calcination treatment.

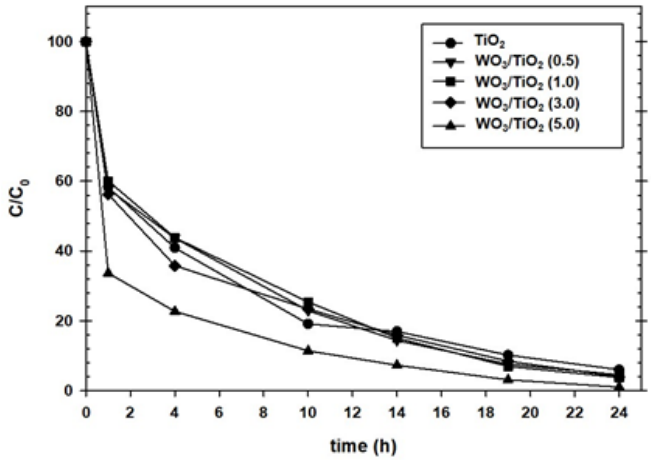

Figure 5. Photocatalytic degradation of methylene blue solution under UV radiation.

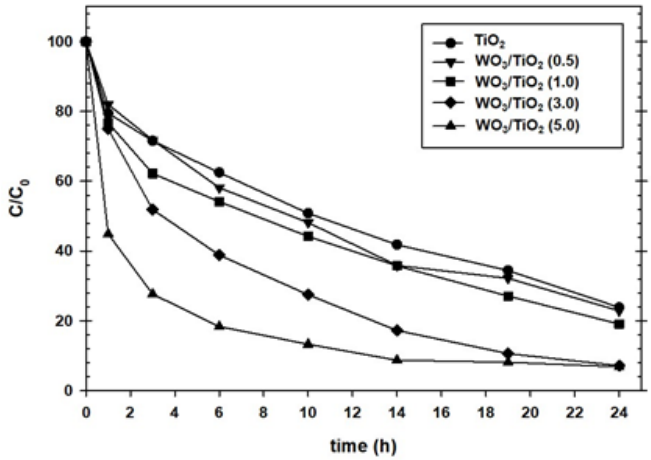

Figure 6. Photocatalytic degradation of methylene blue solution under visible-light radiation.

nanofiber sponges with smooth surface were observed on the $Ti(OBu)_4$/PVP and a series of H_2WO_4/$Ti(OBu)_4$/PVP fiber sponges. The average fiber diameter of $Ti(OBu)_4$/PVP fiber sponges was 430 nm, while the average fiber diameters of 480, 540, 573, and 645 nm were found in H_2WO_4/$Ti(OBu)_4$/PVP fiber sponges at molar percentage ratios of tungsten to Ti of 0.5, 1.0, 3.0, and 5.0, respectively. The increase in fiber diameter observed was due to the increase in the amount of H_2WO_4 loading in the fibers. After calcination treatment (figures on the right column), the average fiber diameters of fibers blown-spun from $Ti(OBu)_4$/PVP precursor solution was 340 nm, while the average fiber diameters of 351, 386, 414, and 479 nm were obtained from H_2WO_4/$Ti(OBu)_4$/PVP precursor solution of tungsten to Ti molar percentage ratios of 0.5, 1.0, 3.0, and 5.0, respectively. The smaller fiber diameters were observed in all cases, suggesting that the removal of PVP occurred during the calcination process.

The nanocomposite fiber sponges containing WO_3 and TiO_2 were further investigated to confirm the presence of WO_3 within by using X-ray diffractometer (XRD). After calcination treatment, hydrate water in H_2WO_4 was released, resulting in the formation of high crystalline WO_3 (Ke et al., 2018). XRD patterns revealed the peaks at 23.1°, 23.6°, and 24.4°, corresponding to the crystal planes (0 0 2), (0 2 0), and (2 0 0) of monoclinic WO_3 (Figure 4). The existence of weak peaks observed at 23.1°, 23.6°, and 24.4° confirmed that WO_3 were successfully formed in the nanocomposite fiber sponges. However, the characteristic peaks of WO_3 were not clearly seen in the nanocomposite fiber sponges with tungsten to Ti molar ratios 0.5 and 1.0 due to the low amounts of WO_3 within.

The photocatalytic activities of nanocomposite fiber sponges consisting of WO_3 and TiO_2 with various molar percentage ratios of tungsten to Ti (i.e., 0.5, 1.0, 3.0, and 5.0), in comparison to the TiO_2 nanofiber sponges, were further evaluated by photocatalytic degradation of methylene blue solution under both UV- and visible-light radiation. In Fig. 5, under UV radiation, the degradation of methylene blue solution using the TiO_2 nanofiber sponges or a series of nanocomposite fiber sponges consisting of tungsten and TiO_2 were observed to increase progressively with increasing UV exposure time. After 1 h of experiment, the concentration of methylene blue was about 60% as found in all samples except nanocomposite fiber sponges at tungsten to Ti molar percentage ratio of 5.0, which was about 33%. After 24 h, the methylene blue solution was almost diminished, especially in nanocomposite fiber sponges at tungsten to Ti molar percentage ratio of 5.0 (about 1% left), while the remaining methylene blue were found in a range of about 4% to 6% for the rest of of photocatalyst samples.

Figure 6 shows the methylene blue degradation profiles of the photocatalysts under visible-light radiation. The photoacatalytic degradation rate of methylene blue solution under visible-light radiation was found to be slower than under UV radiation, however, the similar trend was observed. The photocatalytic degradation performance was found to increase with increasing WO_3 content. Interestingly, WO_3/TiO_3 (5.0) showed significantly higher performance in both UV- and visible light irradiation compared to the others. A sharp decrease in methylene blue concentration (around 55 -65%) was observed in the first hour. The faster degradation of methylene blue observed under UV radiation might be ascribed to the fact that the photogenerated electrons from TiO_2 could be transfer to the conduction band of WO_3 under UV radiation, leading to an increase in the lifetime of the photogenerated electrons and holes (Luevano-Hipolito et al., 2014).

Conclusion

Visible-light photocatalyst nanocomposite fiber sponges were successfully prepared from tungsten trioxide (WO_3) and titanium dioxide (TiO_2) by solution blow-spinning process. After calcination treatment, hydrate water of H_2WO_4 within nanocomposite fiber sponges was removed, resulting in formation of high crystalline WO_3. The presence of WO_3/TiO_2 at tungsten/Ti molar ratio of 5.0 showed the best photocatalytic performance in degradation of methylene blue solution under both UV- and visible-light radiation.

References

Chakornpradit, P., Phiriyawirut, M., & Meeyoo, V. (2017) Preparation of TiO2/WO_3 Composite Nanofibers by Electrospinning. Key Engineering Materials, 751, 296-301.

Chen, Z., Zhao, J., Yang, X., Ye, Q., Huang, K., Hou, C., Zhao, Z., You, J., & Li, Y. (2016) Fabrication of TiO_2/WO_3 composite nanofibers by electrospinning and photocatalystic performance of the resultant fabrics. Industrial & Engineering Chemistry Research, 55, 80-85.

Doshi, J., & Reneker, D. H. (1995) Electrospinning process and applications of electrospun fibers. Journal of Electrostatics, 35, 151–60.

Elahifard, M.R., Rahimnejad, S., Haghighi, S., & Gholami, M.R. (2007) Apatite-coatedAg/AgBr/TiO_2 visible-light photocatalyst for destruction of bacteria. Journal of American Chemical Society, 129, 9552–9553.

Hayden, S.C., Allam, N.K., & El-Sayed, M.A. (2010) TiO_2 nanotube/CdS hybrid electrodes:extraordinary enhancement in the inactivation of Escherichia coli. Journal of American Chemical Society,132, 14406–14408.

Ismail, A.A., & Bahnemann, D.W. (2011) Mesostructured Pt/TiO_2 Nanocomposites as highly active photocatalysts for the photooxidation of dichloroacetic acid. The Journal of Physical Chemistry C, 115, 5784–5791.

Ke, J., Zhou, H., Liu, J., Duan, X., Zhang, H., Liu, S., & Wang, S. (2018) Crystal transformation of 2D tungstic acid H_2WO_4 to WO_3 for enhanced photocatalytic water oxidation. Journal of Colloid and Interface Science, 514, 576–583.

Khil, M. S., Cha, D. I., Kim, H. Y., Kim, I. S., & Bhattarai, N. (2003) Electrospun nanofibrous polyurethane membrane as wound dressing. Journal of Biomedical Materials Research Part B: Applied Biomaterials, 67, 675–679.

Kment, S., Riboni, F., Pausova, S., Wang, L., Wang, L., Han, H., Hubicka, Z., Krysa, J., Schnuki, P., & Zboril, R. (2017) Photoanodes based on TiO_2 and a-Fe2O3 for solar water splitting-superior role of 1D nanoarchitectures and of combined heterostructures, Chemical Society Reviews, 46, 3716–3769.

Laursen, A., Kegnas, S., Dahl, S., & Chorkendorff, I. (2012) Molybdenum sulfides-efficient and viable materials for electro- and photoelectrocatalytic hydrogen evolution, Energy & Environmental Science, 5, 5577–5591.

Li, D., Haneda, H., Hishita, S., & Ohashi, N. (2005) Visible-light-driven N–F–codoped TiO_2 photocatalysts. 2. Optical characterization, photocatalysis, and potential application to air purification. Chemistry of Materials, 17, 2596–2602.

Linsebigler, A.L., Lu, G., & Yates, J.T. (1995) Photocatalysis on TiO_2 surfaces: principles, mechanisms, and selected results, Chemical Reviews, 95, 735-758.

Luevano-Hipolito, E., Martínez-de la Cruz, A., Lopez-Cuellar, E., Yu, Q.L., & Brouwers, H.J.H. (2014) Synthesis, characterization and photocatalytic activity of WO_3/TiO_2 for NO removal under UV and visible light irradiation. Materials Chemistry and Physics, 148, 208–213.

Mugunthan, E., Saidutta, M.B., & Jagadeeshbabu, P.E. (2018) Visible light assisted photocatalytic degradation of diclofenac using TiO_2-WO_3 mixed oxide catalysts. Environmental, Nanotechnology & Monitoring Management, 10, 322-330.

Ofori, A.O., Sheikh, F.A., Appiah-Ntiamoah, R., Yang, X., & Kim, H. (2015) A Simple Method of Electrospun Tungsten Trioxide Nanofibers with Enhanced Visible-Light Photocatalytic Activity. Nano-Micro Letters, 7, 291–297.

Szilagyi, I. M., Santala, E., Heikkilä, M., Pore, V., Kemell, M., Nikitin, T., Teucher, G., Firkala, T., Khriachtchev, L., Räsänen, M., Ritala, M., & Leskelä, M. (2013) Photocatalytic Properties of WO_3/TiO2 core/shell nanofibers prepared by electrospinning and atomic layer deposition. Chemical Vapor Deposition, 19, 149-155.

Wang, H., Zhang, X., Wang, N., Li, Y., Feng, X., Huang, Y., Zhao, C., Liu, Z., Fang, M., Ou, G., Gao, H., Li, X., & Wu, H. (2017) Ultralight, scalable, and high-temperature–resilient ceramic nanofiber sponges. Science Advances, 3, 1–9.

Wang, X.P., & Lim, T.T. (2013) Highly efficient and stable Ag-AgBr/TiO_2 composites for destruction of Escherichia coli under visible light irradiation. Water research, 47, 4148-4158.

Yadav, M., Yadav, A., Fernandes, R., Popat, Y., Orlandi, M., Dashora, A., Kothari, D.C., Miotello, A., Ahuja, B.L., & Patel, N. (2017) Tungsten-doped TiO_2/reduced Graphene Oxide nano-composite photocatalyst for degradation of phenol: A system to reduce surface and bulk electron-hole recombination. Journal of Environmental Management, 203, 364-374.

Ye, L., Pelton, R., Brook, M.A., Filipe, C.D.M., Wang, H.F., Brovko, L., & Griffiths, M. (2013) Targeted disinfection of E. coli via bioconjugation to photoreactive TiO_2. Bioconjugate Chemistry, 24, 448–455.

Zeng, Y., Wu, W., Soowohn, L., & Gao, J.H. (2007) Photocatalytic performance of plasma sprayed Pt-modified TiO_2 coatings under visible light irradiation. Catalalysis Communications, 8, 906–912.

Zhang, X., Fujishima, A., Jin, M., Emeline, A.V., & Murakami, T. (2006) Double-layered TiO_2 –SiO_2 nanostructured films with self-cleaning and antireflective properties. The Journal of Physical Chemistry B, 110, 25142–25148.